



**HAL**  
open science

# Design of Bright Chemogenetic Reporters Based on the Combined Engineering of Fluorogenic Molecular Rotors and of the HaloTag Protein

Justine Coïs, Sylvestre Bachollet, Louis Sanchez, Nicolas Pietrancosta,  
Vincent Vialou, Jean-maurice Mallet, Blaise Dumat

► **To cite this version:**

Justine Coïs, Sylvestre Bachollet, Louis Sanchez, Nicolas Pietrancosta, Vincent Vialou, et al.. Design of Bright Chemogenetic Reporters Based on the Combined Engineering of Fluorogenic Molecular Rotors and of the HaloTag Protein. Chemistry - A European Journal, In press, 10.1002/chem.202400641 . hal-04569035

**HAL Id: hal-04569035**

**<https://hal.science/hal-04569035>**

Submitted on 6 May 2024

**HAL** is a multi-disciplinary open access archive for the deposit and dissemination of scientific research documents, whether they are published or not. The documents may come from teaching and research institutions in France or abroad, or from public or private research centers.

L'archive ouverte pluridisciplinaire **HAL**, est destinée au dépôt et à la diffusion de documents scientifiques de niveau recherche, publiés ou non, émanant des établissements d'enseignement et de recherche français ou étrangers, des laboratoires publics ou privés.

# Design of Bright Chemogenetic Reporters Based on the Combined Engineering of Fluorogenic Molecular Rotors and of the HaloTag Protein

Justine Cois,<sup>[a, b]</sup> Sylvestre P. J. T. Bachollet,<sup>[a]</sup> Louis Sanchez,<sup>[a]</sup> Nicolas Pietrancosta,<sup>[a, b]</sup> Vincent Vialou,<sup>[b]</sup> Jean-Maurice Mallet,<sup>[a]</sup> and Blaise Dumat<sup>\*[a]</sup>

The combination of fluorogenic probes (fluorogens) and self-labeling protein tags represent a promising tool for imaging biological processes with high specificity but it requires the adequation between the fluorogen and its target to ensure a good activation of its fluorescence. In this work, we report a strategy to develop molecular rotors that specifically target HaloTag with a strong enhancement of their fluorescence. The divergent design facilitates the diversification of the structures to tune the photophysical and cellular properties. Four bright fluorogens with emissions ranging from green to red were

identified and applied in wash-free live cell imaging experiments with good contrast and selectivity. A HaloTag mutant adapted from previous literature reports was also tested and shown to further improve the brightness and reaction rate of the most promising fluorogen of the series both *in vitro* and in cells. This work opens new possibilities to develop bright chemogenetic reporters with diverse photophysical and biological properties by exploring a potentially large chemical space of simple dipolar fluorophores in combination with protein engineering.

## Introduction

Chemogenetic reporters associating a genetically-encoded self-labeling protein (SLP) tag and fluorogenic small molecular probes (fluorogens) are a versatile alternative to the use of fluorescent proteins. The genetic encoding of the SLP-tag combined with the fluorogenicity of the probe ensures a high signal specificity, since the excess of fluorogen will remain undetected and, by simply changing the fluorophore, it is possible to tune the color of the reporter, avoiding the cloning and possible optimization of a new recombinant protein. The most commonly used SLP tags are the covalent HaloTag and SNAP-tag but several alternatives exist, including non-covalent strategies.<sup>[1–4]</sup> As for the fluorescent ligands, most of the current research revolves around the rhodamine scaffold. Rhodamine-based fluorogens exploit a reversible spirocyclization reaction: dark aggregated rhodamines in the spirocyclic form open and become fluorescent upon reaction with HaloTag or SNAP-tag.<sup>[5,6]</sup> First limited to silarhodamines, the strategy has been adapted

to various rhodamine scaffolds with diverse emission wavelengths and to cyanine dyes.<sup>[7–9]</sup> This approach benefits from the brightness and photostability of the rhodamine or cyanine derivatives but it relies on complex multistep synthetic pathways sometimes involving costly metal-catalyzed couplings.<sup>[10–12]</sup> An alternative is to use environmentally-sensitive probes, such as molecular rotors.<sup>[13,14]</sup> They are dipolar flexible structures that are not fluorescent in the free state due to non-radiative vibrational and rotational decay, but they become fluorescent when their structure is constrained in a viscous environment or when bound to biomacromolecules such as nucleic acids, proteins or membranes.<sup>[15–18]</sup> Small dipolar structures, such as the ones described herein, generally display moderate molar absorption coefficients and fluorescence quantum yields, especially compared to rhodamines or cyanines, but they constitute a valuable alternative with a different activation mechanism and present some undeniable advantages such as their accessibility in straightforward 2 or 3 synthetic steps and their tunability. Molecular rotors indeed encompass a wide chemical space of flexible dipolar structures and their absorption and emission wavelength can be easily tuned by changing the nature of the electron donating or withdrawing groups, or the length of electronic conjugation.<sup>[14,17,19]</sup> Molecular rotor fluorogens have been successfully developed for SNAP-tag,<sup>[20,21]</sup> but HaloTag represents a more promising target. It has a faster reaction rate and its chloroalkane ligand is chemically simpler and more lipophilic, which facilitates the synthesis of the conjugates and improves their cell penetration. We have recently started to explore the development of fluorogenic molecular rotors targeting HaloTag and we have obtained a palette of fluorogens (Halo probes) covering the green to near infra-red (NIR) range that enable wash-free imaging of proteins in live cells.<sup>[19,22]</sup> However, the fluorescence brightness after

[a] J. Cois, Dr. S. P. J. T. Bachollet, L. Sanchez, Dr. N. Pietrancosta, Dr. J.-M. Mallet, Dr. B. Dumat

Laboratoire des biomolécules, LBM, Département de chimie, École normale supérieure, PSL University, Sorbonne Université, CNRS, 75005 Paris, France  
E-mail: blaise.dumat@ens.psl.eu

[b] J. Cois, Dr. N. Pietrancosta, Dr. V. Vialou

Laboratoire Neurosciences Paris Seine, Sorbonne Université, CNRS, INSERM, 75005 Paris, France

Supporting information for this article is available on the WWW under <https://doi.org/10.1002/chem.202400641>

© 2024 The Authors. Chemistry - A European Journal published by Wiley-VCH GmbH. This is an open access article under the terms of the Creative Commons Attribution Non-Commercial License, which permits use, distribution and reproduction in any medium, provided the original work is properly cited and is not used for commercial purposes.

reaction with HaloTag and the contrast in live cell imaging experiment strongly depend on the structure (Figure 1A and Table S1). Molecular modeling and experimental comparison with their properties in glycerol showed that their fluorescence is only partially activated in the HaloTag protein that seems to lack a defined hydrophobic pocket where the Halo probes could bind and be conformationally locked.<sup>[19,22]</sup> Furthermore, the reaction rates observed are in the range of  $10^3 \text{ M}^{-1} \text{ s}^{-1}$ , which is fast but still several orders of magnitude lower than the reaction rate of tetramethylrhodamine (Halo-TMR) with HaloTag7 ( $10^7 \text{ M}^{-1} \text{ s}^{-1}$ ).<sup>[23]</sup> Overall, our previous studies led us to the conclusion that (i) the properties of our Halo probes are structure-dependent and require a careful balance between the photophysical and biological properties to avoid non-specific activation and (ii) HaloTag is not perfectly fitted for molecular rotors with a partial fluorescence activation and moderate reaction rates.

HaloTag was indeed engineered around the rhodamine molecular scaffold up to the last commercial iteration HaloTag7.<sup>[1,24]</sup> Additional engineering for rhodamine-based probes has been recently reported by the Johnsson group to further improve the properties and enable lifetime multiplexing.<sup>[25]</sup> In addition to rhodamines, HaloTag7 is active with a variety of molecules and probes but they do not work as well, displaying in particular lower reaction rates.<sup>[26–29]</sup> Recent reports have however shown that it is possible to engineer the HaloTag protein via rational design or directed evolution to optimize its interaction with scaffolds other than rhodamines such as a styrylpyridinium or benzothiadiazole dyes.<sup>[28,30,31]</sup>

In this work we have thus combined a new molecular rotor design strategy with the engineering of a HaloTag mutant to obtain bright chemogenetic reporters. Seven new fluorogens were obtained using a divergent synthesis that facilitates the structural diversification and enabled both the tuning of the

photophysical properties and the development of cell-excluded probes dedicated to membrane protein imaging. The probes were tested with HaloTag7 and with a HaloTag mutant mHT containing two mutations selected from previous literature reports. Their characterization *in vitro* and in live cells led to the identification of four probes with enhanced fluorescence properties, spanning the green to red emission range. They have been used to image intracellular and membrane proteins with high contrast following simple wash-free protocols. The properties of the brightest probe of the series (brightness and reaction rate) are improved in the presence of mutant mHT both *in vitro* and in cellular imaging experiments.

## Results & Discussion

**Design of the fluorogens.** The previous design strategy was based on a linear construction where the HaloTag linker was coupled to the electron-withdrawing group of the molecular rotors (Figure 1A). This linear construction was inspired by the work of the Kool group on styrylpyridinium structures that are also molecular rotors. Upon reaction with HaloTag, these so-called “channel dyes” are locked in the narrow binding channel of the protein, leading to an increase of their fluorescence.<sup>[27]</sup> In the case of our previously reported Halo probes, molecular modeling calculations have shown that they do not enter the HaloTag binding channel, possibly due to their bent shape and bulkier electron-withdrawing groups, and have only evidenced few interactions with amino-acids on the surface of the protein.<sup>[19,22]</sup> Nonetheless, these surface interactions proved sufficient to activate the fluorescence of the probes, albeit with varying efficacy depending on their structures. Since the properties are very structure-dependent and difficult to predict by theoretical calculations, we have developed a new design

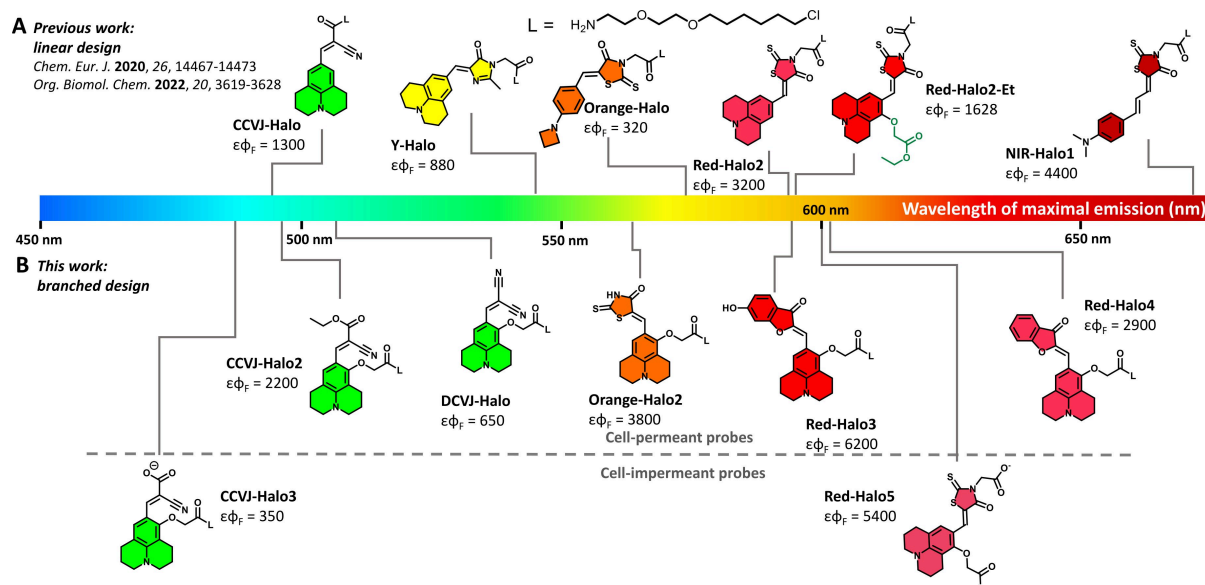


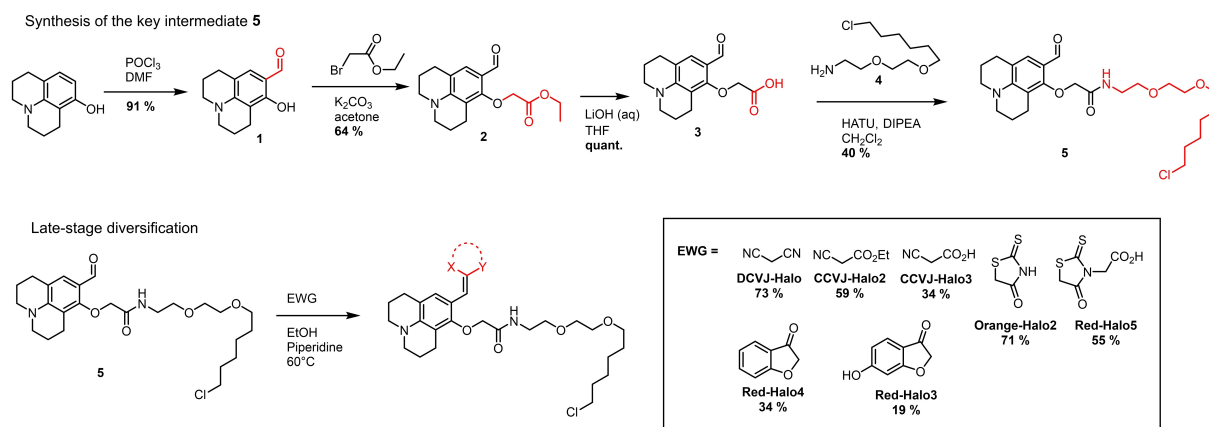
**Figure 1. Design of the Halo probes.** Structures of the previously (A) and newly (B) developed Halo probes with the fluorescence brightness of their complex with the HaloTag protein. Probes are positioned on the visible spectrum according to their maximum emission wavelength.

that facilitates the structural diversification. Since the objective is not to enter the HaloTag binding channel, we have implemented a new branched design where the HaloTag linker is attached directly onto the julolidine moiety. The julolidine moiety was chosen since it increases the fluorescence quantum yield by preventing the formation of a twisted intramolecular charge transfer (TICT) state around the aniline bond.<sup>[22]</sup> It is also a stronger electron donor and induces a bathochromic shift in emission and absorption compared to a dimethylaminobenzyl group. This strategy allows a late-stage diversification in a single step of aldol condensation (Knoevenagel reaction) from one key intermediate **5** (Scheme 1, Figure 1B). The latter can be obtained in good yield in four synthetic steps, starting from 8-hydroxyjulolidine. Whenever two diastereoisomers are possible, only one was isolated and the selectivity is governed by the steric hindrance as shown previously for comparable structures.<sup>[32–34]</sup> A variety of electron-withdrawing groups (EWGs) were tested, including some that were already found in the first generation of Halo probes, such as malononitrile (yielding derivatives of the classical CCVJ and DCVJ rotors,<sup>[32]</sup> **CCVJ-Halo2** and **DCVJ-Halo**) or rhodanine (**Orange-Halo2**). The new design allowed us to introduce a free carboxylic acid function to develop cell-impermeant probes (**CCVJ-Halo3** & **Red-Halo5**) as well as new EWGs based on the benzofuranone scaffold to yield aurone derivatives (**Red-Halo3&4**). Aurones are natural pigments and have been reported to be fluorescent, but this scaffold remains poorly explored in fluorogenic probe design.<sup>[33]</sup>

The molecular rotors on which are built the new Halo probes have been previously studied but the presence of an unusual alkoxy group in the ortho position of the rotating bond may influence their property. As a preliminary evaluation, we have verified that they are indeed viscosity-sensitive fluorophores by comparing their properties in PBS and in PBS with 80% w/v glycerol (Figure S1&S2). All probes are soluble in PBS at least until 10  $\mu$ M and they exhibit a very weak emission. Addition of 80% glycerol results in a slight hyperchromicity and a large increase of fluorescence showing that the HaloTag-targeted molecular rotors retain the viscosity-sensitive emission of their parent structures. It is worth noting also that **Orange-**

**Halo2** and **Red-Halo3** have labile protons on their electron-withdrawing moieties and display pH-sensitive emissions with an increase of fluorescence from acidic to neutral pH and a  $pK_a$  of 7.4 and 7.1 respectively (Scheme S1, Figure S3). This equilibrium overlaps with a second one at very acidic pH due to the protonation of the julolidine amine that is common to all probes but happens outside of the relevant biological pH range. Before characterizing the probes in presence of HaloTag, we also evaluated them in live confocal microscopy of wild-type HeLa cells to assess their potential as fluorogenic probes. Indeed, our experience with the previous generation of Halo probes showed that, despite their high fluorescence enhancements *in vitro*, some probes are prone to non-specific activation in hydrophobic organelles which can significantly reduce the contrast in cellular imaging.<sup>[19]</sup> The non-specific signal of the newly developed probes was thus compared with the previously reported **Red-Halo2** and **Red-Halo2-Et** or with **CCVJ-Halo** depending on their excitation wavelength (Figure S4). **CCVJ-Halo2** and **DCVJ-Halo** give a weak cytoplasmic signal, as was previously observed for **CCVJ-Halo** and **Orange-Halo2** similarly yields a dim signal on par with that of **Red-Halo2-Et** which was specifically developed to minimize the non-specific signal of **Red-Halo2**. The aurone derivatives **Red-Halo3** and in particular **Red-Halo4** give relatively high cytoplasmic signals and, regardless of its photophysical properties, the latter is therefore not expected to be a good fluorogen for wash-free live cell imaging. This first characterization in cells also showed that **CCVJ-Halo3** and **Red-Halo5**, as expected from the presence of a negative charge, likely do not enter cells since no nonspecific signal was observed (data not shown).

**Characterization in HaloTag7.** The properties of the probes were measured in presence of the HaloTag7 protein produced in our laboratory including, for comparison purposes, those of the previously reported probes that were initially tested with a commercial GST-HaloTag protein. Measurements for the first generation of probes are summarized in Table S1 and Figure 1 and gave significantly different results with typically higher quantum yields than previously reported.<sup>[19,22]</sup> The second generation of Halo probes cover the green to red emission range (Figure 2A&B, Table 1) and, as was observed with glycerol,



Scheme 1. Synthesis of the Halo probes

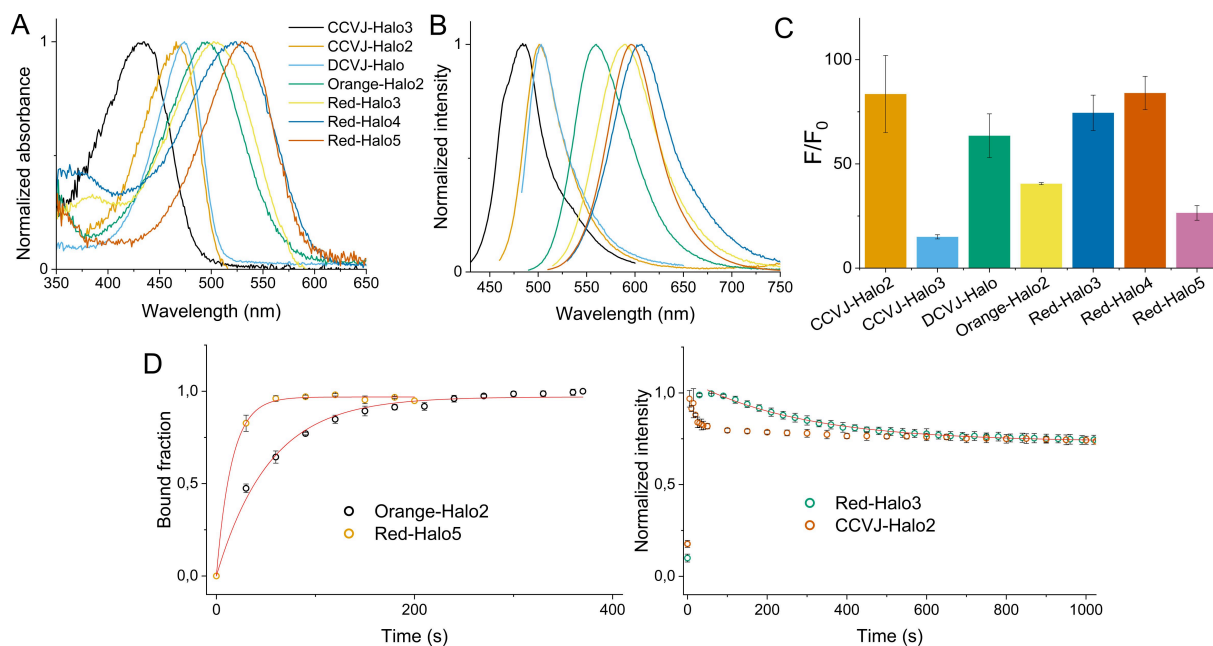


**Figure 2. Characterization of the Halo probes in HaloTag7.** (A) Absorption and (B) fluorescence spectra of the probes in presence of HaloTag7. (C) Fluorescence enhancement factor  $F/F_0$  in presence of HaloTag7.  $F$ : fluorescence of the probe bound to HaloTag7,  $F_0$ : fluorescence of the free probe in PBS. Conditions: 1  $\mu\text{M}$  of probe in PBS with or without 1.5 eq of HaloTag7 protein. Average of two measurements (D) Kinetics of the reaction between the Halo probes and HaloTag7. Data was fitted to a monoexponential function except for CCVJ-Halo2. Average of two measurements.

Molecule	Protein	$\lambda_{\text{abs}}$	$\epsilon$	$\lambda_{\text{em}}$	$\Delta\lambda$	$\phi_F$	$\epsilon\phi_F$	Rel. bright.	$F/F_0$	$k_2^b$ ( $10^3 \text{ M}^{-1}\text{s}^{-1}$ )
CCVJ-Halo2	HaloTag7	466	38800	503	37	0.056	2200	–	84	Nd
	mHT	473 <sup>a</sup>	–	497	24	–	–	0.60	–	–
	PBS	459	21000	498	–	–	–	–	–	–
CCVJ-Halo3	HaloTag7	419	14000	481	62	0.025	350	–	15	–
	PBS	432	13000	493	–	–	–	–	–	–
DCVJ-Halo	HaloTag7	474	31100	503	29	0.021	650	–	64	–
	PBS	469	19000	496	–	–	–	–	–	–
Orange-Halo2	HaloTag7	496	18200	560	64	0.21	3800	–	41	$9.4 \pm 0.40$
	mHT	502 <sup>a</sup>	–	575	73	–	–	0.54	–	–
	PBS	487	20000	590	–	–	–	–	–	–
Red-Halo3	HaloTag7	502	24600	590	88	0.25	6200	–	75	$1.7 \pm 0.022$
	mHT	500 <sup>a</sup>	–	582	82	–	–	1.6	108	$17 \pm 3.0$
	PBS	475	22000	611	–	–	–	–	–	–
Red-Halo4	HaloTag7	523	19500	605	82	0.15	2900	–	84	–
	PBS	493	12200	613	–	–	–	–	–	–
Red-Halo5	HaloTag7	532	34000	600	68	0.16	5400	–	27	$33 \pm 6.0$
	mHT	531 <sup>a</sup>	–	582	51	–	–	0.98	–	–
	PBS	523	32000	608	–	–	–	–	–	–

$\lambda_{\text{abs}}$ : maximum absorption wavelength (nm),  $\epsilon$ : molar absorption coefficient ( $\text{M}^{-1}\text{cm}^{-1}$ ),  $\lambda_{\text{em}}$ : maximum emission wavelength (nm),  $\Delta\lambda$ : Stokes-shift in nm,  $\phi_F$ : fluorescence quantum yield,  $\epsilon\phi_F$ : brightness, rel. bright.: brightness in mHT relative to HaloTag7,  $F/F_0$ : ratio of the fluorescence in the protein with that in PBS,  $k_2$ : second order reaction rate constant. <sup>a</sup> Measured on the excitation spectrum. <sup>b</sup> Average of two independent measurements. Nd: not determined.

their fluorescence can be activated by reaction with HaloTag with up to 84-fold fluorescence enhancements (Figure 2C). The two probes bearing a free carboxylate function, **CCVJ-Halo3** and **Red-Halo5**, display significantly lower increases of

fluorescence due to their stronger residual fluorescence in water that can be attributed to their higher hydrophilicity and also to the low brightness in the case of **CCVJ-Halo3**.

As we observed in our previous studies, the efficiency of the HaloTag fluorescence activation is highly structure-dependent with unpredictable effects (Figure 1, Table 1). In 80% glycerol aqueous solution all three derivatives of the CCVJ and DCVJ rotors exhibited comparable fluorescence intensities (Figure S2) but in presence of HaloTag **CCVJ-Halo3** and **DCVJ-Halo** both display a low brightness and were not further studied. The new design otherwise led to the identification of brighter probes in the green (**CCVJ-Halo2**), Orange (**orange-Halo2**) and red (**Red-Halo3**) range compared to the first generation and to a bright cell-excluded probe with a red emission (**Red-Halo5**). The benzofuranone EWG in particular yielded two of the brightest HaloTag complexes of the series with a red emission (**Red-Halo3&4**). These results confirm previous reports suggesting that the aurone scaffold is promising for the development of bright push-pull dipolar fluorophores.<sup>[33,35,36]</sup> However, while **Red-Halo4** may be a good fluorogen for other applications, its high non-specific signal measured in confocal microscopy prevents its use in cellular imaging and it was not characterized in more details (see above and Figure S4). We next assessed the reaction kinetics of the four most promising probes (**CCVJ-Halo2**, **Orange-Halo2** and **Red-Halo3&5**) with HaloTag by following the increase of fluorescence intensity during the reaction in pseudo-first order conditions (20 equivalents of protein) (Figure 2D). **Red-Halo5** and **Orange-Halo2** yield an expected increase of fluorescence that could be fitted to a monoexponential function to calculate the second order rate constants while **Red-Halo3** and **CCVJ-Halo2** yield a biphasic reaction curve. Such a behavior was already observed for Y-Halo and can be attributed to a two-step reaction mechanism where the probe first non-covalently associate to HaloTag before forming the covalent bond.<sup>[37]</sup> In the case of **CCVJ-Halo2** the second phase is too fast to be fitted, but for **Red-Halo3** it was possible to extract the reaction rate constant corresponding to the covalent step (Table 1). The newly designed probes react faster than the previous ones with reaction rate constants one order of magnitude higher in the range of  $10^4 \text{ M}^{-1} \text{ s}^{-1}$  except for **Red-Halo3** (Table 1 and Table S1). In the case of **CCVJ-Halo2**, even if the reaction rate constant could not be measured accurately, the reaction is essentially finished after one minute which makes it the fastest reacting probe of the two generations. The new fluorogen design thus afforded four

new probes with emission in the green (**CCVJ-Halo2**), orange (**Orange-Halo2**) and red (**Red-Halo3&5**) ranges with superior photophysical properties and faster reaction rates with HaloTag compared to the first generation.

**Characterization in a HaloTag mutant.** In addition to designing enhanced fluorogens, we also sought to engineer the partner protein to improve the interaction of the two parts of our fluorescent chemogenetic reporters. To that end, we based ourselves on two previous literature reports of HaloTag engineering. Miro-Vinyals *et al.* engineered HaloTag for a styrylpyridinium “channel dye” by rational design, ending up with a mutant, HaloTag-SP5, with three mutations M175Y/V245A/L271D that shows increased brightness and reaction rate.<sup>[31]</sup> The effect of the L271D mutation was attributed to an electrostatic interaction with the pyridinium and seems very specific to this structure, but the mutation of methionine 175 was also previously reported to increase the reaction rate of HaloTag with unrelated dansyl derivatives.<sup>[28]</sup> In both papers, the substitution of M175 is shown to open more widely the HaloTag binding channel and speed up the reaction, which suggests that this mutation may work well with a variety of structures. According to a recent preprint, the directed evolution of HaloTag7 to optimize its interaction with a benzothiadiazole dye also led to the identification of mutation V245A, which also supports the choice of this mutation as a generally applicable one.<sup>[30]</sup> Given the similar viscosity-based activation mechanism that our Halo probe share with the “channel dye”, we have thus chosen, as a starting point, to keep the two mutations M175Y/V245A to design a HaloTag mutant mHT.

The brightest probes in the two generations of Halo dyes were tested in presence of mHT and their fluorescence compared to that observed with HaloTag7 (Figure 3, Figure S5).

The mHT mutant activates the fluorescence of our Halo probes, giving comparable spectral properties than in HaloTag7 with only minor shifts in excitation or emission wavelength observed for **Orange-Halo2** and **Red-Halo5** (Table 1, Figure 3 and Figure S5). However, the brightnesses are generally lower than in HaloTag7 with one exception, as **Red-Halo3** exhibits a 64% increase of fluorescence (Figure 3A). We next monitored the reaction kinetics of **Red-Halo3** with mHT and, in contrast to HaloTag7, observed a classical growing curve (Figure 3C, Fig-

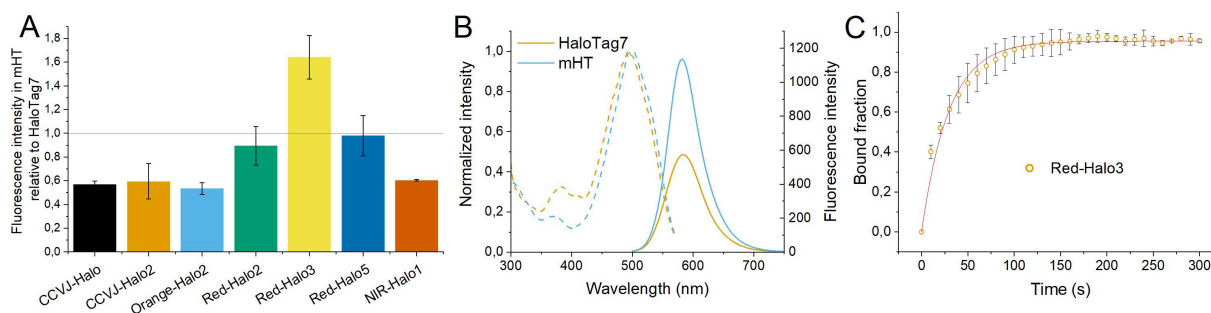


**Figure 3. characterization of the Halo probes in mHT.** (A) Fluorescence of the fluorogens in presence of mHT relative to their fluorescence in presence of HaloTag7. Average of two measurements. (B) Excitation spectra (normalized, dashed lines) and emission spectra (full lines) of Red-Halo3 in HaloTag7 and mHT. (C) Kinetics of the reaction between Red-Halo3 and mHT. Data was fitted to a monoexponential function. Average of two measurements.

ure 2D). Even if this difference in behavior does not facilitate the comparison, the measured reaction rate constant of **Red-Halo3** with mHT is one order of magnitude higher than in HaloTag7 (Table 1). To elucidate the origin of the improved brightness of **Red-Halo3** in mHT, we performed 10 ns molecular dynamics on its complexes with HaloTag7 and mHT. The results show that **Red-Halo3** forms a more stable complex with mHT compared to HaloTag7 with a strong  $\pi$ - $\pi$  interaction between the benzofuranone moiety and the mutated tyrosine (Figure 4A&B). The analysis of the root mean square fluctuations (RMSF) of the atoms of the fluorophore moiety and of the HaloTag linker show that both part are less mobile in the mutant, consistent with a better immobilization of the rotor and thus a better fluorescence activation. RMSF analysis of the binding pocket also show a lower mobility during the dynamics, consistent with a more stable mHT/Red-Halo3 complex. The two mutations appear to create a tighter binding pocket since, counterintuitively, the smaller alanine 245 allows the  $\alpha$  helix containing the tyrosine 175 to fold more tightly by occupying the freed space, creating more constraints on the positioning of Red-Halo3, particularly on the HaloTag linker part (Figure 4D and Figure S6). These results confirm that these two mutations play a key role in the reaction with HaloTag, even though they are not as generally applicable as expected.

## Live Cell Microscopy

We next assessed the performances of the four most promising probes in confocal imaging of live-cell transfected with

HaloTag7 or mHT proteins. To evaluate the imaging contrast, we first imaged live HeLa cells expressing a HaloTag7-NLS protein and incubated with 0.5  $\mu$ M of Halo probe to measure the ratio  $S/NS$  between the specific signal  $S$  in the nuclei and the non-specific cytoplasmic signal  $NS$  without any washing step or medium change (Figure 5A). To compensate for variations in protein expression levels, we analyzed a large number of cells (> 100 cells for each probe) and the distribution of the results is given on Figure 5B. The three probes efficiently stain the nuclei of transfected cells, giving bright and contrasted images in wash-free imaging protocols. **CCVJ-Halo2**, that showed very little non-specific activation in wild-type cells exhibits a very good selectivity with a mean  $S/NS$  ratio of 10. **Red-Halo3** and **Orange-Halo2** exhibit comparable contrast (mean  $S/NS=7$ ) showing that the brightness of **Red-Halo3** partially compensate for its more important nonspecific signal (see above and Figure S4). The probes also proved to be efficient in staining actin as well as cytoplasmic organelles demonstrated here with the Golgi apparatus (Figure 5C&D). To evidence the importance of the contrast, we also tested **Red-Halo4** in wash-free imaging and the results confirm that, despite its good *in vitro* properties, it is not suitable for wash-free imaging due to a strong off-target activation (Figure S7). It is worth noting that for cytoplasmic proteins the nonspecific signal will inevitably interfere more strongly than for the nuclear labeling and the quality of wash-free imaging results may depend on the nature of the protein and on its expression level.

**Red-Halo5**, with its free carboxylic acid function, did not cross the cell membrane and no signal was measured in HeLa

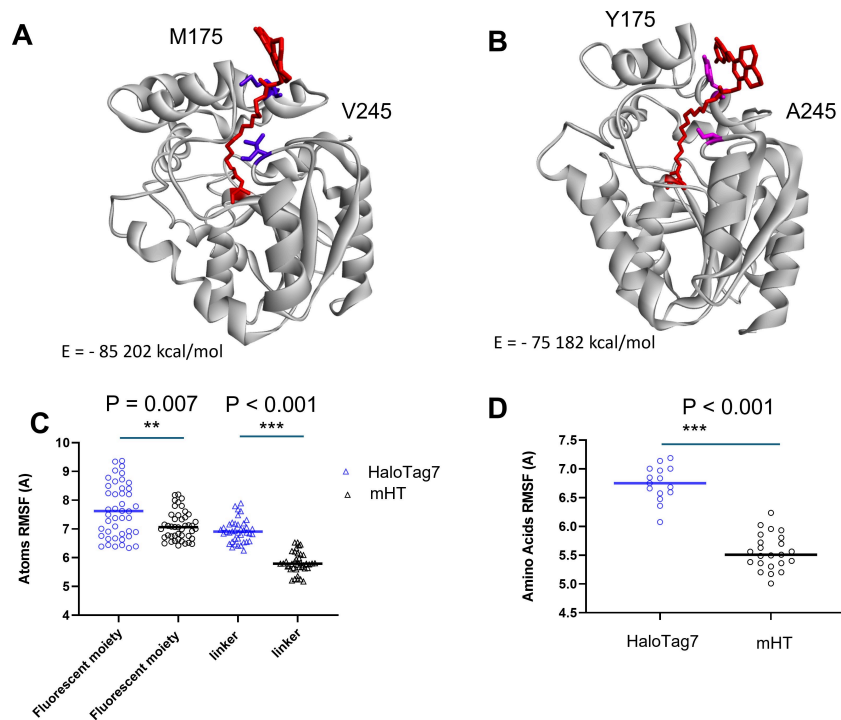


**Figure 4.** Molecular dynamics of HaloTag7 and mHT complexed with Red-Halo3. Representative conformations and associated energies of Red-Halo3 (in red) in HaloTag7 (A) and mHT (B), mutated residues are highlighted in blue and purple. (C) root-mean square fluctuations (RMSF) of the atoms in the fluorophore and HaloTag linker parts of Red-Halo3. (D) RMSF of the amino-acids in the binding pocket (within 4 Å distance to Red-Halo3).

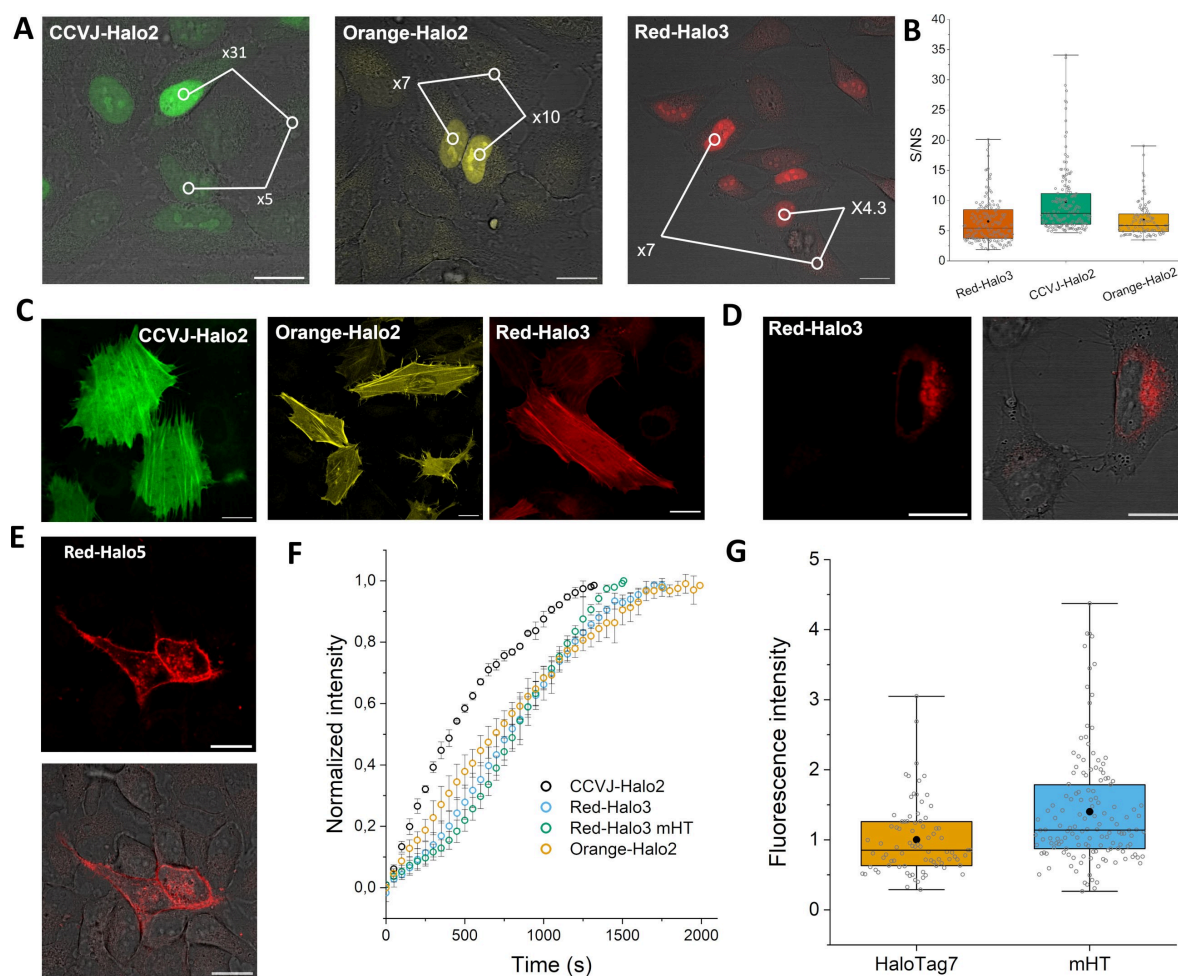


**Figure 5. Properties of the Halo probes in live-cell imaging.** (A) Merged confocal microscopy and brightfield images of live HeLa cells transiently transfected with HaloTag7-NLS and incubated with 0.5  $\mu\text{M}$  of Halo probe in wash-free conditions. On each panel is shown the contrast ratio between the nuclear and cytoplasmic signal for two cells. (B) Distribution of the contrast ratios measured for Red-Halo3 (N = 147), CCVJ-Halo2 (N = 158) and Orange-Halo2 (N = 99). Box and whiskers plot of the *S/NS* ratio measured for N cells in three independent experiments. *S*: specific nuclear signal and *NS*: non specific cytoplasmic signal (C) Confocal microscopy images of live HeLa cells transiently transfected with HaloTag7-LifeAct and stained with 0.5  $\mu\text{M}$  of Halo probe as indicated on each panel. (D) Confocal microscopy imaging of HeLa cells transiently transfected with Golgi-HaloTag7 and stained with 0.5  $\mu\text{M}$  of Red-Halo3. (left) fluorescence and (right) merged fluorescence and brightfield images. (E) Confocal microscopy imaging of live HeLa cells transiently transfected with PDGFR-HaloTag7 and stained with 0.5  $\mu\text{M}$  of Red-Halo5. (top) fluorescence and (bottom) merged fluorescence and brightfield images. (F) Labeling kinetics in live HeLa cells transfected with HaloTag7-NLS or mHT-NLS where indicated. Fluorescence intensity measured every 10 s after addition of the probes in the nucleus of N cells from two independent experiments. CCVJ-Halo2 (N = 3), Orange-Halo2 (N = 4), Red-Halo3 (N = 5), Red-Halo3@mHT (N = 5). (G) Relative fluorescence intensity of live HeLa cells transfected with either HaloTag7-NLS (N = 82) or mHT-NLS (N = 142). Mean fluorescence intensity measured in the nuclei of N cells from two independent experiments and normalized to the mean value of HaloTag7-NLS.

cells either wild-type or transfected with cytoplasmic or nuclear proteins (data not shown). It could however efficiently be used to label the PDGFR-HaloTag7 membrane protein with excellent selectivity (Figure 5E). Such cell-impermeant probes are preferable for staining membrane proteins since they avoid non-specific cytoplasmic signal and any intracellular signal can safely be attributed to membrane recycling and endosome formation.<sup>[38]</sup>

The labeling kinetics of the probes were assessed in HeLa cells transfected with HaloTag7-NLS (Figure 5F). In agreement with the reaction rate constants measured *in vitro*, **CCVJ-Halo2** reacts the fastest ( $t_{1/2} = 6.8$  min) followed by **Orange-Halo2** ( $t_{1/2} = 11.5$  min). The labeling curve of **Red-Halo3** shows two stages, with an initial lag phase followed by a more rapid increase of fluorescence. Our hypothesis, supported by the higher cytoplas-

mic signal measured in wild-type cells, is that **Red-Halo3** has a higher affinity for cytoplasmic organelles than its counterparts, which temporarily delays its reaction with HaloTag and explains the initial lag phase. Finally, we tested the performance of the mHT mutant in cellular imaging by targeting a mHT-NLS protein. All three cell-permeant probes exhibit a similar nuclear labeling as observed with HaloTag7-NLS, showing that the mHT protein is active in cells (Figure S8). In agreement with the *in vitro* measurements, **Red-Halo3** is brighter in cells transfected with mHT-NLS with a 40% increase on average (Figure 5G). No such increase of brightness is observed for **CCVJ-Halo2** or **Orange-Halo2** with mHT (Figure S9), which confirms that this improvement is indeed linked to the formation of a brighter complex between **Red-Halo3** and mHT and not for instance to a higher expression level of mHT. The labeling kinetics of mHT

with Red-Halo3 in cells is similar to that of HaloTag7: although it seems that, after the lag phase, the reaction is slightly faster with mHT, the difference does not appear to be significant (Figure 5F).

The newly developed Halo probes are thus efficient for imaging HaloTag fusion proteins in live cells, yielding bright and contrasted images in wash-free conditions thanks to their fluorogenicity. Except for the cell-excluded Red-Halo5, they penetrate cells and react with HaloTag rapidly with labeling times that correlate well with the reaction rates measured *in vitro*. Cellular imaging experiments also confirm the improvement of the brightness of Red-Halo3 in the mHT mutant.

## Conclusions

The molecular design strategy described herein enabled the enhancement of the photophysical properties and reaction rates of the Halo fluorogens and led to the discovery of three fluorogenic probes that can be used in combination with HaloTag to replace green- (CCVJ-Halo2), orange- (Orange-Halo2) or red-emitting (Red-Halo3) fluorescent proteins. Cell-excluded Red-Halo5 was also developed for the specific labeling of membrane proteins. In cells expressing HaloTag fusion proteins, they yield bright and contrasted images with the simplest imaging protocol: add the probe and image after a 15 to 30 minutes incubation time. A first attempt at engineering HaloTag7 by selecting, from previous literature reports, two mutations that seemed applicable to our molecular rotors led to a mutant mHT that improves the brightness and reaction rate of Red-Halo3 both *in vitro* and in cells, opening new possibilities to further improve our hybrid fluorescent reporters. This work shows that it is possible to develop bright HaloTag-targeted fluorogens based on simple molecular rotor structures. However, the large variability of the photophysical and cellular properties observed even for molecules with only minor structural differences such as Red-Halo3&4 makes it difficult to establish clear guidelines for their future design. We anticipate that simple design strategies, such as the one described here, will enable the rapid exploration of a large chemical space and help identify adequate probes. This molecular chemistry approach should also be coupled to more powerful protein engineering techniques such as directed evolution to optimize the interaction of the two partners.

## Acknowledgements

This work was supported by the Agence Nationale de la Recherche (ANR-18-CE44-0006). JC is supported by a PhD fellowship funded by the “interface pour le vivant” (IPV) initiative of Sorbonne Université.

## Conflict of Interests

The authors have no conflict of interest to declare.

## Data Availability Statement

The data that support the findings of this study are available from the corresponding author upon reasonable request.

- [1] G. V. Los, L. P. Encell, M. G. McDougall, D. D. Hartzell, N. Karassina, C. Zimprich, M. G. Wood, R. Learish, R. F. Ohana, M. Urh, D. Simpson, J. Mendez, K. Zimmerman, P. Otto, G. Vidugiris, J. Zhu, A. Darzins, D. H. Klaubert, R. F. Bulleit, K. V. Wood, *ACS Chem. Biol.* **2008**, *3*, 373–382.
- [2] A. Keppler, S. Gendreizig, T. Gronemeyer, H. Pick, H. Vogel, K. Johnsson, *Nat. Biotechnol.* **2003**, *21*, 86–9.
- [3] M.-A. Plamont, E. Billon-Denis, S. Maurin, C. Gauron, F. M. Pimenta, C. G. Specht, J. Shi, J. Quéard, B. Pan, J. Rossignol, K. Moncoq, N. Morellet, M. Volovitch, E. Lescop, Y. Chen, A. Triller, S. Vriz, T. Le Saux, L. Jullien, A. Gautier, *Proc. Nat. Acad. Sci.* **2016**, *113*, 497–502.
- [4] C. Jing, V. W. Cornish, *Acc. Chem. Res.* **2011**, *44*, 784–92.
- [5] G. Lukinavičius, L. Reymond, K. Umezawa, O. Sallin, E. D'Este, F. Göttfert, H. Ta, S. W. Hell, Y. Urano, K. Johnsson, *J. Am. Chem. Soc.* **2016**, *138*, 9365–9368.
- [6] J. Zhang, H. Shi, C. Huang, L. Mei, Q. Guo, K. Cheng, P. Wu, D. Su, Q. Chen, S. Gan, C. K. Wing Chan, J. Shi, J. L. Chen, C. H. Jonathan Choi, S. Q. Yao, X. Chen, B. Z. Tang, J. He, H. Sun, *ACS Nano* **2023**, *17*, 3632–3644.
- [7] S. M. Usama, S. C. Marker, D. Li, D. R. Caldwell, M. Stroet, N. L. Patel, A. G. Tebo, S. Hernot, J. D. Kalen, M. Schnermann, *J. Am. Chem. Soc.* **2023**, *145*, 14647–14659.
- [8] L. Wang, M. Tran, E. D'Este, J. Roberti, B. Koch, L. Xue, K. Johnsson, *Nat. Chem.* **2020**, *12*, 165–172.
- [9] H. Ohno, E. Sasaki, S. Yamada, K. Hanaoka, *Org. Biomol. Chem.* **2024**, DOI 10.1039/d4ob00130c.
- [10] J. B. Grimm, A. N. Tkachuk, R. Patel, S. T. Hennigan, A. Gutu, P. Dong, V. Gandin, A. M. Osowski, K. L. Holland, Z. J. Liu, T. A. Brown, L. D. Lavis, *J. Am. Chem. Soc.* **2023**, *145*, 23000–23013.
- [11] J. B. Grimm, T. A. Brown, A. N. Tkachuk, L. D. Lavis, *ACS Cent. Sci.* **2017**, *3*, 975–985.
- [12] J. Bučevičius, R. Gerasimaitė, K. A. Kiszka, S. Pradhan, G. Kostiuk, T. Koenen, G. Lukinavičius, *Nat. Commun.* **2023**, *14*, 1306.
- [13] A. S. Klymchenko, *Acc. Chem. Res.* **2017**, *50*, 366–375.
- [14] S. C. Lee, J. Heo, H. C. Woo, J. A. Lee, Y. H. Seo, C. L. Lee, S. Kim, O. P. Kwon, *Chem. A Eur. J.* **2018**, *24*, 13706–13718.
- [15] T. Mukherjee, R. J. Martinez-sanchez, K. T. Fam, S. Bou, L. Richert, D. Garnier, Y. Me, S. Kanvah, A. S. Klymchenko, Y. Mély, S. Kanvah, A. S. Klymchenko, M. Collot, *Mater. Chem. Front.* **2021**, *5*, 2459–2469.
- [16] W. L. Goh, M. Y. Lee, T. L. Joseph, S. T. Quah, C. J. Brown, S. Verma, S. Brenner, F. J. Ghadessy, Y. N. Teo, *J. Am. Chem. Soc.* **2014**, *136*, 6159–6162.
- [17] S. Ye, H. Zhang, J. Fei, C. H. Wolstenholme, X. Zhang, *Angew. Chem. Int. Ed.* **2021**, *60*, 1339–1346.
- [18] W. T. Yu, T. W. Wu, C. L. Huang, I. C. Chen, K. T. Tan, *Chem. Sci.* **2016**, *7*, 301–307.
- [19] S. P. J. T. Bachollet, Y. Shpinov, F. Broch, H. Benaissa, A. Gautier, N. Pietrancosta, J.-M. Mallet, B. Dumat, *Org. Biomol. Chem.* **2022**, *20*, 3619–3628.
- [20] D. Zhang, Z. Chen, Z. Du, B. Bao, N. Su, X. Chen, Y. Ge, Q. Lin, L. Yang, Y. Hua, S. Wang, X. Hua, F. Zuo, N. Li, R. Liu, L. Jiang, C. Bao, Y. Zhao, J. Loscalzo, Y. Yang, L. Zhu, *Cell Discov.* **2023**, *9*, 56.
- [21] K. H. Jung, M. Fares, L. S. Grainger, C. H. Wolstenholme, A. Hou, Y. Liu, X. Zhang, *Org. Biomol. Chem.* **2019**, *17*, 1906–1915.
- [22] S. P. J. T. Bachollet, C. Addi, N. Pietrancosta, J.-M. Mallet, B. Dumat, *Chem. A Eur. J.* **2020**, *26*, 14467–14473.
- [23] L. P. Encell, R. F. Ohana, K. Zimmerman, P. Otto, G. Vidugiris, M. G. Wood, G. V. Los, M. G. McDougall, C. Zimprich, N. Karassina, R. D. Learish, R. Hurst, J. Hartnett, S. Wheeler, P. Stecha, J. English, K. Zhao, J. Mendez, H. A. Benink, N. Murphy, D. L. Daniels, M. R. Slater, M. Urh, A. Darzins, D. H. Klaubert, R. F. Bulleit, K. V. Wood, *Curr. Chem. Genomics* **2012**, *6*, 55–71.
- [24] L. P. Encell, *Curr. Chem. Genomics* **2012**, *6*, 55–71.
- [25] M. S. Frei, M. Tarnawski, M. J. Roberti, B. Koch, J. Hiblot, K. Johnsson, *Nat. Methods* **2022**, *19*, 65–70.
- [26] B. J. Lampkin, J. A. Kritzer, *Chem. Commun.* **2024**, *60*, 200–203.
- [27] S. A. Clark, V. Singh, D. Vega Mendoza, W. Margolin, E. T. Kool, *Bioconjugate Chem.* **2016**, *27*, 2839–2843.

- [28] M.-G. Kang, H. Lee, B. H. Kim, Y. Dunbayev, J. K. Seo, C. Lee, H.-W. Rhee, *Chem. Commun.* **2017**, *53*, 9226–9229.
- [29] Y. Liu, K. Miao, N. P. Dunham, H. Liu, M. Fares, A. K. Boal, X. Li, X. Zhang, *Biochemistry* **2017**, *56*, 1585–1595.
- [30] B. J. Lampkin, B. J. Goldberg, J. A. Kritzer, *bioRxiv* **2023**, DOI 10.1101/2023.10.29.564634.
- [31] C. Miró-Vinyals, A. Stein, S. Fischer, T. R. Ward, A. Deliz Liang, *ChemBioChem* **2021**, *22*, 3398–3401.
- [32] T. Iwaki, C. Torigoe, M. Noji, M. Nakanishi, *Biochemistry* **1993**, *32*, 7589–7592.
- [33] N. Shanker, O. Dilek, K. Mukherjee, D. W. McGee, S. L. Bane, *J. Fluoresc.* **2011**, *21*, 2173–2184.
- [34] C. Li, M. Plamont, I. Aujard, T. Le Saux, L. Jullien, A. Gautier, *Org. Biomol. Chem.* **2016**, *14*, 9253–9261.
- [35] M. Ono, Y. Maya, M. Haratake, K. Ito, H. Mori, M. Nakayama, *Biochem. Biophys. Res. Commun.* **2007**, *361*, 116–121.
- [36] M. Y. Guo, L. G. Wei, J. W. Shen, X. J. Liu, M. Abbas, Y. S. Yang, C. Xu, B. Z. Wang, H. L. Zhu, *Dyes Pigm.* **2022**, *202*, 110261.
- [37] S. M. Marques, M. Slanska, K. Chmelova, R. Chaloupkova, M. Marek, S. Clark, J. Damborsky, E. T. Kool, D. Bednar, Z. Prokop, *JACS Au* **2022**, *2*, 1324–1337.
- [38] R. Birke, J. Ast, D. A. Roosen, J. Lee, K. Roßmann, C. Huhn, B. Mathes, M. Lisurek, D. Bushiri, H. Sun, B. Jones, M. Lehmann, J. Levitz, V. Haucke, D. J. Hodson, J. Broichhagen, *Org. Biomol. Chem.* **2022**, *20*, 5967–5980.

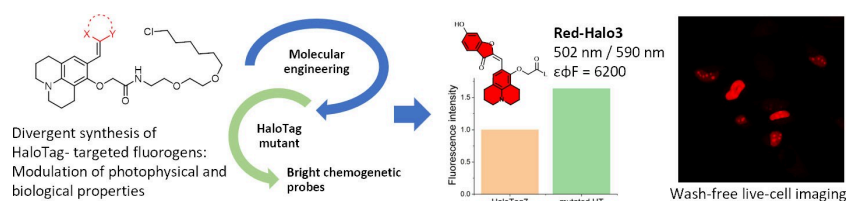
---

Manuscript received: February 16, 2024

Accepted manuscript online: April 4, 2024

Version of record online: ■■, ■■

# RESEARCH ARTICLE



A series of bright chemogenetic reporters based on the HaloTag technology with green to red emission range were obtained by combining the molecular engineering of chemically-accessible fluorescent molecular

rotors with mutations of the HaloTag protein. The reporters are suitable for wash-free live cell imaging with good contrast and the design strategy facilitates the future diversification and optimization of the properties.

*J. Cois, Dr. S. P. J. T. Bachollet, L. Sanchez, Dr. N. Pietrancosta, Dr. V. Vialou, Dr. J.-M. Mallet, Dr. B. Dumat\**

1 – 10

## Design of Bright Chemogenetic Reporters Based on the Combined Engineering of Fluorogenic Molecular Rotors and of the HaloTag Protein

